PRAMANA
— journal of
physics

Vol. 75, No. 5
November 2010
pp. 855–867

Super-resolution by pupil plane phase filtering

L N HAZRA* and N REZA
Department of Applied Optics and Photonics, University of Calcutta, 92 A.P.C. Road, Kolkata 700 009, India
*Corresponding author
E-mail: lnhaphy@caluniv.ac.in; nasrin.reza.cu@gmail.com

Abstract. Resolution capability of any optical imaging system is limited by residual aberrations as well as diffraction effects. Overcoming this fundamental limit is called super-resolution. Several new paradigms for super-resolution in optical systems use '*a posteriori*' digital image processing. In these ventures the three-dimensional point spread function (PSF) of the lens plays a key role in image acquisition. A straightforward tailoring of the PSF can be performed by appropriate pupil plane filtering. With a brief review of the state-of-art in this research area, this paper dwells upon the inverse problem of global optimization of the pupil function by phase filtering in accordance with the desired PSF.

Keywords. Super-resolution; high-resolution imaging; pupil plane filtering; phase filters; global optimization; evolutionary programming; genetic algorithm.

PACS Nos 07.60.Pb; 42.30.-d; 87.64.-t; 87.57.cf

1. Introduction

The capability of an optical imaging system to image minute details of an object is limited by several factors. The residual aberrations of the imaging lens severely affect its resolving power. Even for an aberration-free objective, diffraction effects arising out of finite aperture of the imaging objective pose a fundamental limit for the least resolvable distance in the object/image. The Rayleigh/Abbe limit on transverse resolution stipulates that $\Delta\xi$, the least resolvable distance on the object/image space is proportional to $(\lambda/n\sin\alpha)$, where $(n\sin\alpha)$ is the object/image space numerical aperture of the imaging objective and λ is the operating wavelength [1]. For three-dimensional objects, assuming complete absence of aberrations for all object–image conjugates, often the above limit for transverse resolution cannot be achieved in practice in the image of a specific transverse section of the object, because of the overlap of the out-of-focus images of other sections of the object on the image. This overlap causes loss in resolution and contrast in the desired transverse image. Again, assuming aberration-free imaging over the longitudinal range of the three-dimensional image, the diffraction limit for the axial or longitudinal resolution stipulates that $\delta\zeta$, the least resolvable distance along the axis,

is proportional to $\lambda/(n \sin \alpha)^2$ [2]. It should be noted that both $\Delta\xi$ and $\delta\zeta$ are affected significantly in the presence of residual aberrations of the imaging lens.

In Fourier optics terminology the above limits are related to the upper limit of spatial frequency in the object/image [3]. Object information above this cut-off frequency is irretrievably lost in the process of image formation. Indeed, in image formation, higher frequency contents of the object are propagated through evanescent waves. The amplitudes of these evanescent waves decrease to an insignificant level after propagating a few wavelengths from the object, and hence is not present in the image.

In order to overcome the fundamental limits in resolution, scanning microscopy techniques are now being increasingly used. For two-dimensional imaging, near-field scanning optical microscopy (NSOM) uses recording of the diffracted pattern at a distance, which is of the order of the working wavelength, the limiting resolution being determined by the lateral size of the scanning spot [4]. Confocal microscopy for imaging transverse sections of three-dimensional objects uses a two-stage imaging process that uses pinholes for reducing blurs caused by out-of-focus images [5]. Recent advances in confocal microscopy, e.g. 4-Pi microscopes, make ingenious use of dual objectives for capturing the evanescent waves also for increasing the lateral resolution further in the desired section [6]. On the other hand, non-point scanning techniques, e.g. nonlinear structured illumination microscopy are also being investigated for capturing information in the object beyond the cut-off frequency [7]. All these techniques extensively uses computer-aided digital image processing techniques. One of their primary goals is to overcome the inherent diffraction limits of optical image formation, and so, they are called techniques for super-resolution.

It is important to remember that the three-dimensional point spread function of the objective plays a key role in determining image quality both in scanning microscopy and non-scanning whole-field microscopy. Pupil plane filtering of the microscope objective provides a straightforward means for achieving different types of point spread functions. In telescopic imagery and spectroscopy, the so-called 'apodizing' and 'super-resolving' filters are used for different image quality improvement purposes. In these applications no attempt is made to cross the fundamental diffraction limit, but 'apodizing' filters are used to increase the low-frequency response of the system allowing a decrease of the high-frequency response, and 'super-resolving' filters increase the high-frequency response along with a decrease in low-frequency response [8–10].

About half a century ago, Toraldo di Francia [11], and subsequently Boivin [12] initiated investigations on pupil plane filtering for exceeding resolution of the imaging system beyond the diffraction limit by using a set of concentric amplitude and/or phase filters on the pupil of an image forming system. For an aberration-free objective, the two-dimensional point spread function, which is called the Airy pattern, consists of a central lobe surrounded by a set of dark and bright rings of gradually decreasing intensity, and the shape of the central lobe effectively determines the least resolvable distance. Central obscuration on the pupil can make the central lobe sharper, but concomitantly this is associated with decrease in intensity in the centre of the diffraction pattern and increase in intensity of the neighbouring side lobes. Thus the apparent gain in resolution obtained by reduction in size of the central lobe is offset by the increase in intensity of the side lobes. By using pupil

with an array of concentric annuli, the point spread function can be tailored in a fashion such that a narrow central lobe is surrounded by neighbouring lobes of low intensity, with one or more lobes of high intensity spaced far away from the centre. Such PSF in scanning microscopy allows use of pinholes of smaller size obtaining significant gain in resolution. In whole-field microscopy, such filters can provide super-resolution beyond the diffraction limit over a small field, size of which is determined by how far apart the large side lobes are located.

Current exigencies in burgeoning application areas like optical data storage, optical micromanipulation and high-resolution imaging have aroused considerable interest in super-resolution in real time. Incidentally, it may be noted that the techniques for super-resolution, mentioned earlier, are 'non-real time' operations.

Recently, many methods for designing super-resolving pupil filters have been proposed, and many researchers have investigated different types of super-resolution filters [13–30]. Although many of these filters aim at transverse super-resolution, some of these are now directed towards axial super-resolution for catering to practical problems that call for high resolution along the longitudinal direction of the optical axis of the imaging system. Indeed, it is possible to tailor the 3D structure of the point spread function by using appropriate pupil plane filters. On the other hand, different types of filters, e.g. a continuous or piece-wise continuous variation of amplitude and/or phase of the pupil plane filters are also being explored for the purpose. Liu and Wang [31] and Tan *et al* [32] have reported the application of global optimization algorithms in designing super-resolving phase filters.

In this paper, we report some of our investigations on the design of piece-wise continuous phase filters. In order to explore globally or quasi-globally the optimum solutions for the problem we use an adaptation of evolutionary programming. The next section presents a mathematical formulation for the fast and accurate evaluation of the PSF parameters. Our evaluation method uses a novel approach for numerical evolution of oscillatory integrals. Section 3 deals with a brief description of our adaptation of evolutionary programming for the purpose. Illustrative results for optimum phase filters are given in §4. Section 5 presents concluding remarks.

2. Mathematical formulation

2.1 *Axial intensity and local variance of wave aberration*

For a circularly symmetric pupil with uniform amplitude the complex amplitude on the axis of the focal plane (figure 1) is given by

$$F_N(0) = 2\int_0^1 \exp[ikW(r)]r\,\mathrm{d}r, \tag{1}$$

where $W(r)$ is the wavefront aberration on the exit pupil of the imaging system, the variable r is a fractional coordinate for a point on the pupil and $k = (2\pi/\lambda)$ is the propagation constant. Changing the variable from r to $t = r^2$,

$$F_N(0) = \int_0^1 \exp[ikW(t)]\mathrm{d}t \tag{2}$$

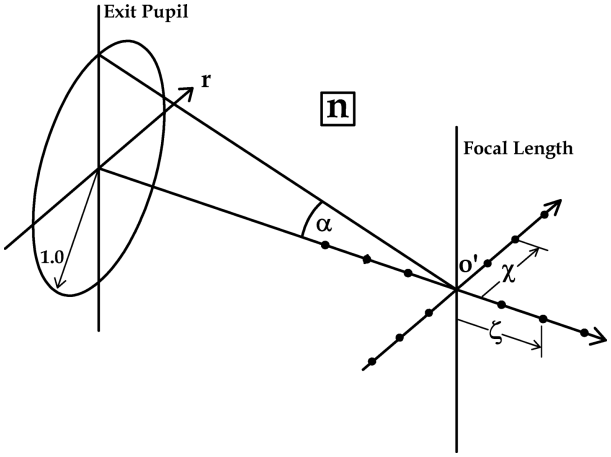

Figure 1. Image space of an imaging system.

$F_N(0)$ represents the normalized axial amplitude in the PSF, and is given by

$$F_N(0) = \frac{F(0)}{F_0(0)}, \tag{3}$$

where $F(0)$ is the actual amplitude of the aberrated system and $F_0(0)$ is the amplitude of an unaberrated system of the same numerical aperture.

For small aberrations, by neglecting terms of degree 3 and above in the Taylor series expansion of the integrand in integral (2), $F_N(0)$ can be approximated as

$$F_N(0) = \left[1 - \frac{k^2}{2}(\overline{W^2} - \overline{W}^2)\right], \tag{4}$$

where

$$\overline{W^2} = \int_0^1 [W(t)]^2 \mathrm{d}t \tag{5}$$

and

$$\overline{W} = \int_0^1 W(t) \mathrm{d}t. \tag{6}$$

$(\overline{W^2} - \overline{W}^2)$ is called the variance of wave aberration of the axially symmetric pupil.

For larger values of wave aberration, expression (4) will yield incorrect results. But, by a modification of expression (4) using local variances over subzones instead of total variance over (0,1), a convenient expression that remains valid for larger values of aberrations can be obtained [33].

Assuming N subzones in t-space, $F_N(0)$ can be written as

$$F_N(0) = 2\varepsilon \sum_{p=1}^{N} \left[1 - \frac{k^2}{2}(\overline{W_p^2} - \overline{W}_p^2)\right] \exp(ik\overline{W}_p), \tag{7}$$

where width of each subinterval $= 2\varepsilon = (1-0)/N = 1/N$, N = total number of subintervals.

$$\overline{W_p^2} = \frac{1}{2\varepsilon}\int_{t_p-\varepsilon}^{t_p+\varepsilon}[W(t)]^2 \mathrm{d}t \tag{8}$$

$$\overline{W}_p = \frac{1}{2\varepsilon}\int_{t_p-\varepsilon}^{t_p+\varepsilon} W(t)\mathrm{d}t. \tag{9}$$

The pth subinterval has inner and outer radii of $(t_p-\varepsilon)$ and $(t_p+\varepsilon)$ respectively where

$$t_p = \frac{(2p-1)}{2N}. \tag{10}$$

$(\overline{W_p^2} - \overline{W}_p^2)$ is the local variance of wave aberration over the pth subinterval. The normalized intensity on the axis is given by the squared modulus of $F_N(0)$ as

$$I_N(0) = 4\varepsilon^2 \sum_{p=1}^{N}\sum_{q=1}^{N}\left[1-\frac{k^2}{2}(\overline{W_p^2}-\overline{W}_p^2)\right] \times\left[1-\frac{k^2}{2}(\overline{W_q^2}-\overline{W}_q^2)\right]\cos[k(\overline{W}_p-\overline{W}_q)]. \tag{11}$$

Axial intensity on transverse plane that is longitudinally shifted by $\Delta\zeta$ from the paraxial focal plane can be determined by considering this shift as defect of focus aberration $W(r) = W_{20}r^2$. W_{20} is related to $\Delta\zeta$ by

$$W_{20} = \frac{1}{2n}(n\sin\alpha)^2\Delta\zeta \tag{12}$$

$(n\sin\alpha)$ is the numerical aperture of the imaging system and n is the refractive index of the image space [34].

In t-space, $W(t) = W_{20}t$. From eqs (8) and (9) we obtain

$$\overline{W_p^2} = \frac{W_{20}^2(3t_p^2+\varepsilon^2)}{3} \tag{13}$$

$$\overline{W}_p = W_{20}t_p. \tag{14}$$

Therefore, the axial intensity on the defocussed image plane is given by

$$I_N(0) = 4\varepsilon^2\left[1-\frac{\varepsilon^2}{6}(kW_{20})^2\right]^2\sum_{p=1}^{N}\sum_{q=1}^{N}\cos[kW_{20}(t_p-t_q)]. \tag{15}$$

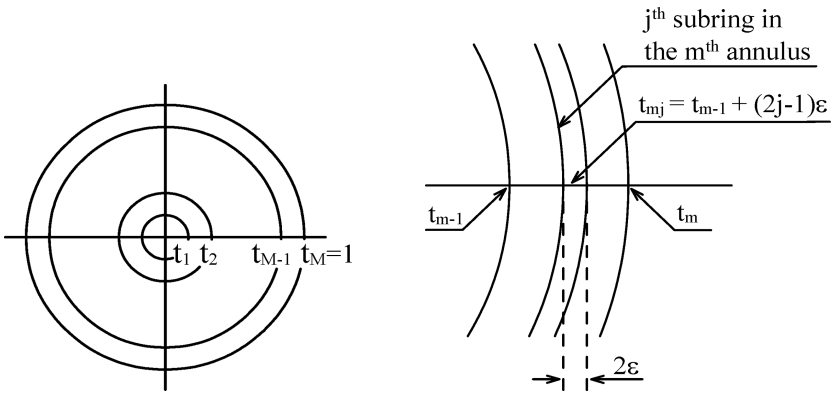

Figure 2. In t-space (**a**) an M-zone concentric equal area phase filter. (**b**) jth subring in the mth equal area annular zone.

2.2 *Axial intensity with concentric multizone equal area phase filters*

A concentric equal area phase filter with M annular zones (figure 2a) can be represented in t-space as

$$Q(t) = \sum_{m=1}^{M} Q_m B_m(t) \tag{16}$$

where $B_m(t)$ are zero-one or Walsh block functions [26],

$$\begin{aligned} B_m(t) &= 1, \quad \text{for } t_{m-1} \le t \le t_m \\ &= 0, \quad \text{otherwise.} \end{aligned} \tag{17}$$

Suppose each phase ring is subdivided into J concentric subrings (figure 2b). For the jth subring, the inner and outer radii in t-space are $(t_{mj} - \varepsilon)$ and $(t_{mj} + \varepsilon)$ respectively. Each subring with $t_m = m/M$ for $m = 1, 2, \ldots, M$ of width 2ε.

$$2\varepsilon = \frac{(t_m - t_{m-1})}{J} = \frac{1}{MJ} = \frac{1}{N}. \tag{18}$$

For defocus W_{20} with a phase filter $Q(t)$, the pupil function is given by

$$f(t) = \exp[ikW(t)], \tag{19}$$

where

$$W(t) = Q(t) + W_{20}t = \sum_{m=1}^{M} Q_m \overline{B}_m(t) + W_{20}t. \tag{20}$$

Consequently, with concentric M-zone phase filter, the normalized axial amplitude on a transverse plane corresponding to defocus W_{20} is given by

$$F_N(0) = 2\varepsilon \sum_{m=1}^{M} \sum_{j=1}^{J} \exp(ik\overline{W}_{mj}) \left[1 - \frac{k^2}{2}(\overline{W_{mj}^2} - \overline{W}_{mj}^2)\right], \tag{21}$$

where $\overline{W}_{mj}$, the average value of $W(t)$ over the jth subring of the mth zone of M-zone phase filter, is given from eq. (20) as

$$\overline{W}_{mj} = Q_m + W_{20} t_{mj}. \tag{22}$$

$(\overline{W_{mj}^2} - \overline{W}_{mj}^2)$ is the local variance of $W(t)$ over the jth subring of the mth zone of the M-zone phase filter. From eq. (20), $\overline{W_{mj}^2}$ is given by

$$\overline{W_{mj}^2} = Q_m^2 + 2Q_m W_{20} t_{mj} + \frac{W_{20}^2(3t_{mj}^2 + \varepsilon^2)}{3}. \tag{23}$$

Substituting from eqs (22) and (23) in eq. (20), we obtain

$$F_N(0) = 2\varepsilon \left[1 - \frac{\varepsilon^2}{6}(kW_{20})^2\right] \sum_{m=1}^{M} \sum_{j=1}^{J} \exp[i\{(kQ_m) + (kW_{20})t_{mj}\}]. \tag{24}$$

The normalized axial intensity corresponding to the M-zone phase filter is given by

$$I_N(0) = 4\varepsilon^2 \left[1 - \frac{\varepsilon^2}{6}(kW_{20})^2\right]^2 \sum_{m=1}^{M} \sum_{j=1}^{J} \sum_{l=1}^{M} \sum_{p=1}^{J} \cos[(kQ_m) - (kQ_l)] + [(kW_{20})(t_{mj} - t_{lp})]. \tag{25}$$

For a given M-zone phase filter, the accuracy in numerical computation of $I_n(0)$ for large value of $\Delta\zeta$ can be improved by increasing the integral value for J.

2.3 *Far-field diffraction pattern in the transverse plane*

In an axially symmetric pupil (figure 1) the far-field amplitude distribution is given by

$$F(p) = \int_0^1 f(r) J_0(pr) r \, \mathrm{d}r, \tag{26}$$

where the reduced diffraction variable p for points on the transverse plane is defined as

$$p = \frac{2\pi}{\lambda}(n \sin\alpha)\chi. \tag{27}$$

χ is the geometrical distance of the point from the axis.

For a uniform transmittance Airy pupil,

$$\begin{aligned} f(r) &= 1, \quad \text{for } 0 \le r \le 1 \\ &= 0, \quad \text{otherwise.} \end{aligned} \tag{28}$$

So, from eq. (26) we get

$$F(p) = \int_0^1 J_0(pr) r \, \mathrm{d}r \tag{29}$$

and

$$F(0) = \int_0^1 r \, \mathrm{d}r = \frac{1}{2}. \tag{30}$$

The normalized amplitude $F_N(p)$ is given by

$$F_N(p) = \frac{F(p)}{F(0)} = \left[\frac{2J_1(p)}{p}\right]. \tag{31}$$

Now considering a concentric equal area phase filter with M number of annular zones, let

$$f(r) = \sum_{m=1}^{M} f_m B_m(r), \tag{32}$$

where $B_m(r)$ are zero-one or Walsh block functions as defined earlier in eq. (17).

Assume the upper and lower radii of the jth annular ring to be r_m and r_{m-1} respectively. The values of these two parameters are as follows:

$$r_m = \left[\frac{m}{M}\right]^{1/2} \quad \text{and} \quad r_{m-1} = \left[\frac{m-1}{M}\right]^{1/2}. \tag{33}$$

Then eq. (31) becomes,

$$\begin{aligned} F_N(p) = \frac{F(p)}{F(0)} &= 2\sum_{m=1}^{M} f_m \int_0^1 \overline{B}_m(r) J_0(pr) r \, \mathrm{d}r \\ &= 2\sum_{m=1}^{M} f_m \int_{r_{m-1}}^{r_m} J_0(pr) r \, \mathrm{d}r. \end{aligned} \tag{34}$$

This can be expressed as

$$F_N(p) = 2\sum_{m=1}^{M} f_m \Im_m(p) \tag{35}$$

where $\Im_m(p)$ denotes

$$\Im_m(p) = \left[\frac{r_m J_1(pr_m) - r_{m-1} J_1(pr_{m-1})}{p}\right]. \tag{36}$$

In the case of phase filters having the same phase kW_m over the mth zone,

$$f_m = \mathrm{e}^{ikW_m}. \tag{37}$$

Substituting from eq. (37) in eq. (35), we obtain

$$F_N(p) = 2\sum_{m=1}^{M} \mathrm{e}^{ikW_m}\Im_m(p). \tag{38}$$

The normalized transverse intensity distribution corresponding to the M zone phase filter is given by

$$I_N(p) = |F_N(p)|^2 = 4\sum_{m=1}^{M}\sum_{n=1}^{M}[\cos\{k(W_m - W_n)\}]\Im_m(p)\Im_n(p). \tag{39}$$

3. Optimum phase filters by evolutionary programming

In the present work the implementation of evolutionary programming is an adaptation of genetic algorithm [35,36]. This consists of binary coding of the design variables, an initial population of randomly generated chromosomes or bit strings and evolution of this population through many generations by successive applications of the three genetic operations, namely, selection, cross-over and mutation. In this algorithm, each individual in a population is assigned a unique fitness value Φ, and the algorithm aims to maximize this fitness in the members of the population in successive generations.

Fitness function Φ is inversely related to the merit function ψ by

$$\Phi = \frac{1}{1+\psi}. \tag{40}$$

The merit function ψ is defined as the weighted sum of axial or transverse intensities at a pre-specified set of regularly space axial or transverse points.

$$\psi = \sum_{d=1}^{D} \omega_d I_d, \tag{41}$$

where I_d is the intensity at the dth point on the axis and ω_d is the corresponding weight. Preferred intensity variations are expected to be obtained by suitable choice of relative values of the weighting factors ω_d.

For the case of M concentric zone equal area phase filters the available number of degrees of freedom is $(M-1)$. Having zero phase to any one of the zones, each of the remaining zones is allowed a finite number P of discrete phase levels over the domain $(0, 2\pi)$. Thus a particular zone can have any phase out of the P phase levels 0, $2\pi/P$, $4\pi/P$, …, $(P-1)2\pi/P$. We implement binary coding of the variables.

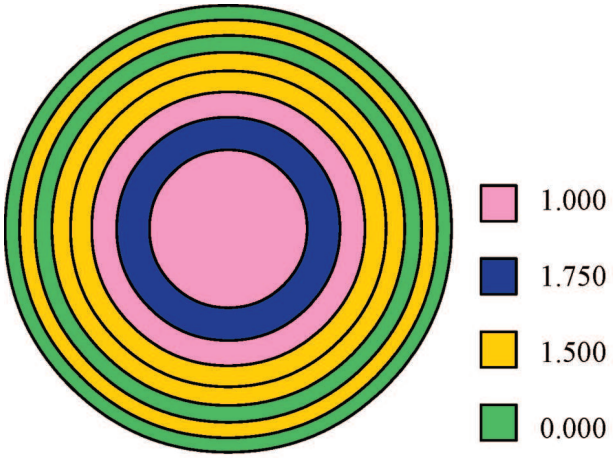

Figure 3. Optimum eight zone concentric equal area axial phase filter.

3.1 *Dynamic merit function*

In order to avoid undue stagnation and slow convergence of the algorithm we experimented with 'dynamic merit function' by redefining the merit function, and correspondingly the fitness function, after each iteration. For the initial population, merit function is taken as the sum of axial or transverse intensities at 99 points corresponding to a in 0.1 (0.1) 10.0. Here a denotes the normalized axial or transverse coordinate, depending on the problem at hand.

In subsequent generations the fittest member of the earlier generation is retained as a member of population of the next generation (elitism). A check on genetic diversity [37] of the population is undertaken and in the case of low diversity, the population is reinitialized, retaining only the elite member. The merit function ψ is redefined as weighted sum of intensities over equidistant points in three regions along the longitudinal or transverse axis. ψ is given by

$$\psi = \sum_{d=1}^{D_1-1} \omega_1 I_d + \sum_{d=D_1}^{D_2} \omega_2 I_d + \sum_{d=D_2+1}^{D_2+5} \omega_3 I_d. \tag{42}$$

Three different weighting factors ω_1, ω_2 and ω_3 are applied for axial or transverse points lying in the three regions along a. The three regions consist of the central lobe, neighbouring side lobes with low intensity and region of high intensity lying beyond the second zone. During the evolutionary process, the shapes of these regions change, and values of D_1, D_2 and the weighting factors ω_1, ω_2 and ω_3 are to be appropriately varied in composition of the merit function. The evolutionary process is affected significantly by the choice of weighting factors. Numerical checks can show that, in general, convergence is ensured when $\omega_1 > \omega_2 > \omega_3$. Details on this stochastic optimization procedure are given in ref. [38].

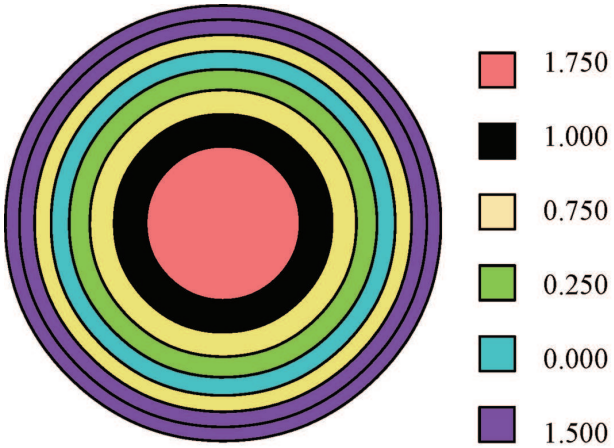

Figure 4. Optimum eight zone concentric equal area transverse phase filter.

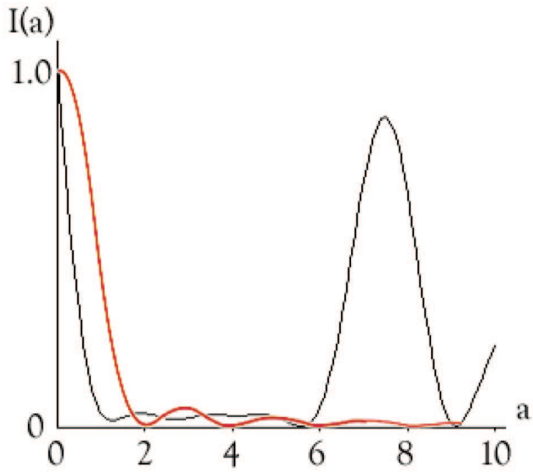

Figure 5. Normalized axial distribution of intensity for the phase filter of figure 3. (Black curve) optimum eight zone concentric equal area phase filter; (red curve) uniform pupil.

4. Illustrative results

The evolutionary programming approach elucidated above for synthesising multi-zone equal area concentric phase filters has been applied to obtain optimum phase filters for axial as well as transverse super-resolution. As an illustrative example, figures 3 and 4 respectively show the pictorial representations for two concentric equal area eight zone phase filters, one each for super-resolution in the axial direction and in the transverse direction. Figures 5 and 6 give the axial intensity distribution and the transverse intensity distribution for the two filters respectively. For comparison, the normalized intensity distributions for the Airy pupil are given

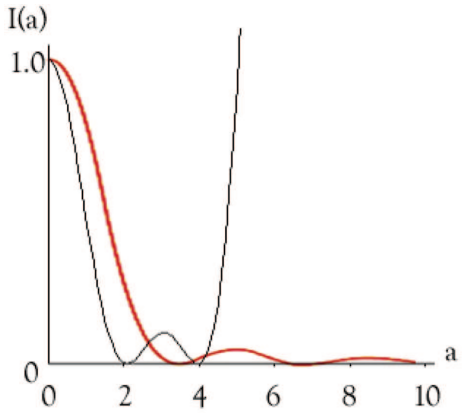

Figure 6. Normalized transverse distribution of intensity for the phase filter of figure 5. (Black curve) optimum eight zone concentric equal area phase filter; (red curve) uniform pupil.

in red. In the optimization procedure for both these filters, each of the eight zones was allowed eight distinct phase levels. The transverse super-resolving filter shown in figure 3 uses only four phase levels out of the allowed eight levels. On the other hand, the axial super-resolving filter uses six phase levels out of the allowed eight levels.

5. Concluding remarks

It is significant to observe that the optimum phase filters obtained by evolutionary programming do not use all discreet phase levels permitted in zones for these equal area multilevel phase filters in both axial and transverse phase filters. This observation validates the conjecture that there are practical upper limits in both the number of zones and the number of allowable phase levels in the synthesis of super-resolving filters, beyond which no significant gain in resolution can be obtained. Undeniably, unequal area multizone phase filters have many more effective degrees of freedom. Investigations on such filters with prescribed programming approach are in progress.

Acknowledgements

Authors are grateful to the University Grants Commission, India for sponsoring a research project during the tenure of which this work is done. Thanks are due to S Pal for his help in carrying out the computations.

References

[1] M Born and E Wolf, *Principles of optics* (Pegramon, Oxford, 1980)
[2] M Gu, *Advanced optical imaging theory* (Springer-Verlag, Berlin, 1999)

[3] J W Goodman, *Introduction to Fourier optics*, 2nd edn (McGraw-Hill, Singapore, 1996)
[4] M A Paesler and P J Moyer, *Near-field optics: Theory, introduction, and applications* (John Wiley, New York, 1996)
[5] T Wilson and C J R Sheppard, *Theory and practice of scanning optical microscopy* (Academic, London, 1984)
[6] http://www.leica-microsystems.com
[7] M G L Gustafsson, *PNAS* **102(37)**, 13081 (2005)
[8] P Jacquinot and B Rozien-Dossier, '*Apodisation*' *in progress in optics* edited by E Wolf (North-Holland, Amsterdam, 1964) 3rd edition
[9] M De, L N Hazra and P Sengupta, *Opt. Acta* **22**, 125 (1975)
[10] L N Hazra, *Opt. Commun.* **21(2)**, 232 (1977)
[11] G Toraldo di Francia, *Atti Fond. Giorgio Ronchi.* **7**, 366 (1952)
[12] A Boivin, *Théorie el Calcul des Figs de Diffraction de Révolution* (Université de Laval, Quebec, 1964)
[13] C J R Sheppard and Z S Hegedus, *J. Opt. Soc. Am.* **A5**, 643 (1988)
[14] M M Corral, P Andrés and J Ojeda-Castaneda, *Appl. Opt.* **33(11)**, 2223, (1994)
[15] M Martínez-Corral, P Andrés, J Ojeda-Castañeda and G Saavedra, *Opt. Commun.* **119**, 491 (1995)
[16] T R M Sales and G M Morris, *J. Opt. Soc. Am.* **A14(7)**, 1637 (1997)
[17] T R M Sales and G M Morris, *Opt. Commun.* **156**, 227 (1998)
[18] C J R Sheppard, M D Sharma and A Arbouet, *Optik* **111**, 347 (2000)
[19] M Martínez-Corral, M T Caballero, E H K Stelzer and J Swoger, *Opt. Express* **10(1)**, 98 (2002)
[20] M P Cagigal, J E Oti, V F Canals and P J Valle, *Opt. Commun.* **241**, 249 (2004)
[21] S Ledesma, J Campos, J C Escalera and M J Yzuel, *Opt. Lett.* **29(9)**, 932 (2004)
[22] H Luo and C Zhou, *Appl. Opt.* **43(34)**, 6242 (2004)
[23] M Yun, L Liu, J Sun and D Liu, *J. Opt. Soc. Am.* **A22**, 272 (2005)
[24] S Ledesma, J C Escalera, J Campos and M J Yzuel, *Opt. Commun.* **249**, 183 (2005)
[25] X Liu, L Liu, D Liu and L Bai, *Optik* **117**, 453 (2006)
[26] L N Hazra, *MICRON* **38**, 129 (2007)
[27] P V Valle, J E Oli, V F Canales and M P Cagigal, *Opt. Commun.* **272**, 325 (2007)
[28] C J R Sheppard, J Campos, J C Escalera and S Ledesma, *Opt. Commun.* **281**, 913 (2008)
[29] C J R Sheppard, J Campos, J C Escalera and S Ledesma, *Opt. Commun.* **281**, 3623 (2008)
[30] T G Jabbour, M Petrovich and S M Kuebler, *Opt. Commun.* **281**, 2002 (2008)
[31] L Liu and G Wang, *Optik* **119**, 481 (2008)
[32] Y Tan, R Guo, S Xiao, G Chang and W Huang, *J. Laser Micro/Nanoengineering* **1**, 281 (2006)
[33] L N Hazra, *Appl. Opt.* **27**, 3464 (1988)
[34] W T Welford, *Aberration of optical systems* (Academic, London, 1986)
[35] I Rechenberg, *Evolutionsstrategie*: *Optimeirung Technischer System nach Prinzipien der Biologischen Evolution* (Frommen-Holzboog Verlag, Stuttgart, 1943)
[36] D E Goldberg, *Genetic algorithm in search, optimization and machine learning* (Addison-Wesley, Reading, 1989)
[37] S Banerjee and L N Hazra, *J. Mod. Opt.* **49**, 7, 1111 (2002)
[38] L N Hazra and N Reza, *Proc. SPIE* **7787**, 77870D-1 (2010)